SANDIA REPORT
SAND2013-8331
Unlimited Release
Printed October 2013

Impeller Deflection and Modal Finite Element Analysis

Nathan A. Spencer

Prepared by
Sandia National Laboratories
Albuquerque, New Mexico 87185 and Livermore, California 94550

Sandia National Laboratories is a multi-program laboratory managed and operated by Sandia Corporation, a wholly owned subsidiary of Lockheed Martin Corporation, for the U.S. Department of Energy's National Nuclear Security Administration under contract DE-AC04-94AL85000.

Approved for public release; further dissemination unlimited.

Sandia National Laboratories

Issued by Sandia National Laboratories, operated for the United States Department of Energy by Sandia Corporation.

NOTICE: This report was prepared as an account of work sponsored by an agency of the United States Government. Neither the United States Government, nor any agency thereof, nor any of their employees, nor any of their contractors, subcontractors, or their employees, make any warranty, express or implied, or assume any legal liability or responsibility for the accuracy, completeness, or usefulness of any information, apparatus, product, or process disclosed, or represent that its use would not infringe privately owned rights. Reference herein to any specific commercial product, process, or service by trade name, trademark, manufacturer, or otherwise, does not necessarily constitute or imply its endorsement, recommendation, or favoring by the United States Government, any agency thereof, or any of their contractors or subcontractors. The views and opinions expressed herein do not necessarily state or reflect those of the United States Government, any agency thereof, or any of their contractors.

Printed in the United States of America. This report has been reproduced directly from the best available copy.

Available to DOE and DOE contractors from
U.S. Department of Energy
Office of Scientific and Technical Information
P.O. Box 62
Oak Ridge, TN 37831

Telephone: (865) 576-8401
Facsimile: (865) 576-5728
E-Mail: reports@adonis.osti.gov
Online ordering: http://www.osti.gov/bridge

Available to the public from
U.S. Department of Commerce
National Technical Information Service
5285 Port Royal Rd.
Springfield, VA 22161

Telephone: (800) 553-6847
Facsimile: (703) 605-6900
E-Mail: orders@ntis.fedworld.gov
Online order: http://www.ntis.gov/help/ordermethods.asp?loc=7-4-0#online

SAND2013-8331
Unlimited Release
October 2013

Impeller Deflection and Modal Finite Element Analysis

Nathan A. Spencer
Multi-Physics Modeling and Simulation

Sandia National Laboratories
7011 East Avenue
Livermore, CA 94551

Abstract

Deflections of an impeller due to centripetal forces are calculated using finite element analysis. The lateral, or out of plane, deflections are an important design consideration for this particular impeller because it incorporates an air bearing with critical gap tolerances. The target gap distance is approximately 10 microns at a rotational velocity of 2500 rpm. The centripetal forces acting on the impeller cause it deflect in a concave fashion, decreasing the initial gap distance as a function of radial position. This deflection is characterized for a previous and updated impeller design for comparative purposes. The impact of design options such as material selection, geometry dimensions, and operating rotational velocity are also explored, followed by a sensitivity study with these parameters bounded by specific design values. A modal analysis is also performed to calculate the impeller's natural frequencies which are desired to be avoided during operation. The finite element modeling techniques continue to be exercised by the impeller design team to address specific questions and evaluate conceptual designs, some of which are included in the Appendix.

ACKNOWLEDGMENTS

The author recognizes Jeff Koplow and Terry Johnson, both in the Energy Systems Engineering and Analysis Department, as the inventor and lead systems integrator, respectively, of the impeller. Funding initially provided by the Laboratory Directed Research and Development (LDRD) program and subsequently by other Department of Energy (DOE) sources provided the resources for this work as well as the system design, prototype fabrication, and testing of the impeller cooling unit.

CONTENTS

1. Introduction 7
2. Spinning disk finite element and analytical comparison 9
3. Impeller design comparison 13
5. Sensitivity / ANOVA Study 21
6. Modal analysis 25
7. Conclusions 27
8. References 29
Appendix A: Version 6 Axial Displacements 31
Appendix B: Impeller Pin Design 33
Appendix C: Thermal Gradient Displacements 35
Distribution 37

FIGURES

Figure 1 Meshes for a simple spinning disk with (a) one (b) two and (c) four elements 9
Figure 2 Analytical and finite element calculated displacements for a spinning disk. 10
Figure 3 Finite element calculated displacements for a spinning disk 10
Figure 4 Displacement contour plot of the spinning disk magnified by a factor of 200,000x. ... 11
Figure 5 Geometry of the version 4 and version 5 impeller designs. 13
Figure 6 Meshed geometry of the version 4 and version 5 impeller designs. 14
Figure 7 Axial displacement contour plots of the version 4 and 5 impeller designs. 15
Figure 8 Comparison of the maximum axial displacement 16
Figure 9 Axial displacements as a function of radial position 16
Figure 10 Parameter trends affecting the impeller gap distance. 18
Figure 11 Zoomed in parameter trends. 18
Figure 12 Plots of each factor colored separately by blue, green, or red 23
Figure 13 Plots of each factor at their low (blue), medium (green), and high (red) levels 24
Figure 14 Version 5 impeller mode shapes and corresponding frequencies. 25
Figure 15 Version 5 (a) isolated fin geometry, (b) first mode, and (c) second mode. 26
Figure 16 Version 6 (a) isolated fin geometry, (b) first mode, and (c) second mode. 26
Figure 17 Meshed geometry of the version 5 and version 6 impeller designs. 31
Figure 18 Maximum axial displacements overlaid with the version 6 impeller design. 32
Figure 19 Meshed geometry of conceptual impeller design with pins forming the fins. 33
Figure 20 Maximum axial displacements overlaid with the pin fin impeller design. 34
Figure 21 Version 5 (a) mapped temperature distribution and (b) resulting axial 35
Figure 22 Axial displacements of the version 5 impeller due to thermal gradients. 36

TABLES

Table 1 Summary of parameter values used in the comparison between the version 4 and 14
Table 2 Summary of parameters and values used in the parameter study.. 17
Table 3 Factor levels selected for a sensitivity study of the axial displacements. 21

1. INTRODUCTION

Design efforts to improve the cooling capacity of an impeller attached to a computer processor are in progress. Part of the design effort includes maintaining a critical gap distance of an air bearing on which the impeller rotates. As the impeller increases in rotational velocity, centripetal forces act upon the impeller. Calculations of the resulting deflections from these forces show that the impeller deflects downward in a concave manner, reducing the air bearing gap. The target gap for the air bearing is currently 10 microns at 2500 rpm. Preliminary calculations indicated that the deflections due to the centripetal forces are close to 10 microns. Therefore, further analysis provided in this report is of interest to the design team to account for the deflections of the impeller.

All of the finite element calculations were performed using the Sierra Structural Mechanics [1] software developed internally at Sandia National Laboratories. Meshes consist of eight node hexahedral elements. The analysis is static with the nodal displacements at the center axle region fixed. The software calculates centripetal forces resulting from rotations about a specified axis and automatically applies them as external forces to all nodes in the mesh.

This report proceeds in the following manner: A simplified model of a spinning disk is first used for comparison to an analytical solution for calculating radial displacements. Next, a comparison of the lateral displacements is made between a previous design and the current one. Then effects of air pressure loads, material selection, and thickness variations are explored. A sensitivity study of the various parameters for a selected design follows. Finally, structural modes of both impeller designs are provided up to 2600 Hz. Additional design questions and conceptual designs are reported in the Appendix.

2. SPINNING DISK FINITE ELEMENT AND ANALYTICAL COMPARISON

A solution for the radial displacements, u(r), of a spinning disk with a central hole is given by [2]:

$$u(r) = \frac{3+}{8} \quad \omega^2 \frac{1-}{E} r \left[a^2 + b^2 - \frac{1+}{3+} r^2 + \frac{1+}{1-} \frac{a^2 b^2}{r^2} \right]$$

where the variables, their descriptions, and assigned values for this problem are listed as:

	Poison's Ratio	0.3
	Density	2.52×10^{-4} lb·s^2/in^4
ω	Rotational velocity in rad/sec	2500 rpm (~261.8 rad/sec)
E	Elastic modulus	10^7 psi
r	Radial position	[0.05 0.25 0.5 0.75 1 1.25 1.5 1.75 2] in
a	Inner radius	0.0455 in
b	Outer radius	2 in

A simple model of the disk was created and meshed with one, two, and four elements through the thickness of the disk for a simple mesh refinement study. The meshes are shown in Figure 1, and the resulting displacements calculated by both the analytical and Sierra Structural Mechanics solutions are shown in Figure 2. The lateral displacements are shown in Figure 3, without an analytical solution for comparison. A contour plot of magnified displacements is shown in Figure 4 to illustrate the thinning effect of the spinning disk.

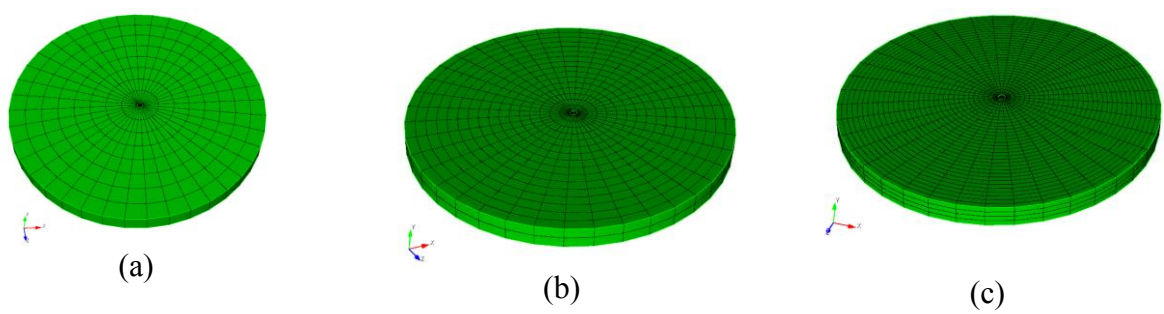

Figure 1 Meshes for a simple spinning disk with (a) one (b) two and (c) four elements through the thickness of the disk.

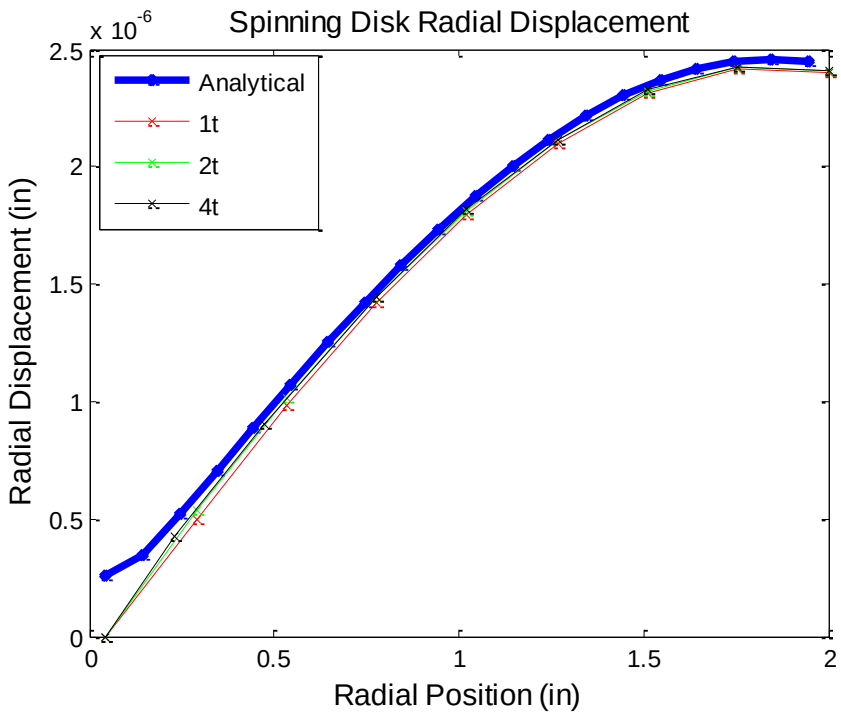

Figure 2 Analytical and finite element calculated displacements for a spinning disk with one (1t), two (2t), and four (4t) elements through the thickness of the disk.

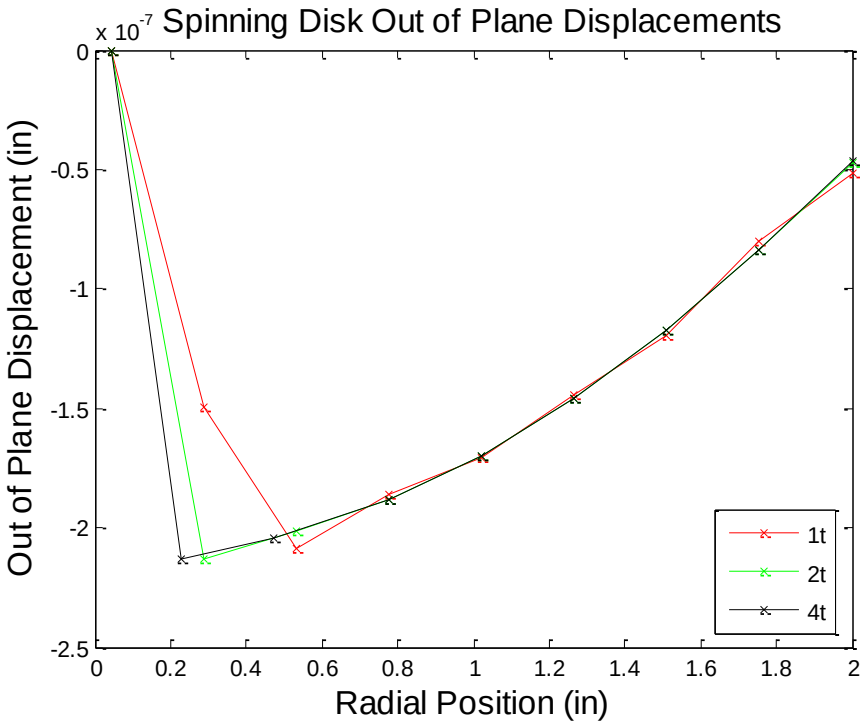

Figure 3 Finite element calculated displacements for a spinning disk with one (1t), two (2t), and four (4t) elements through the thickness of the disk.

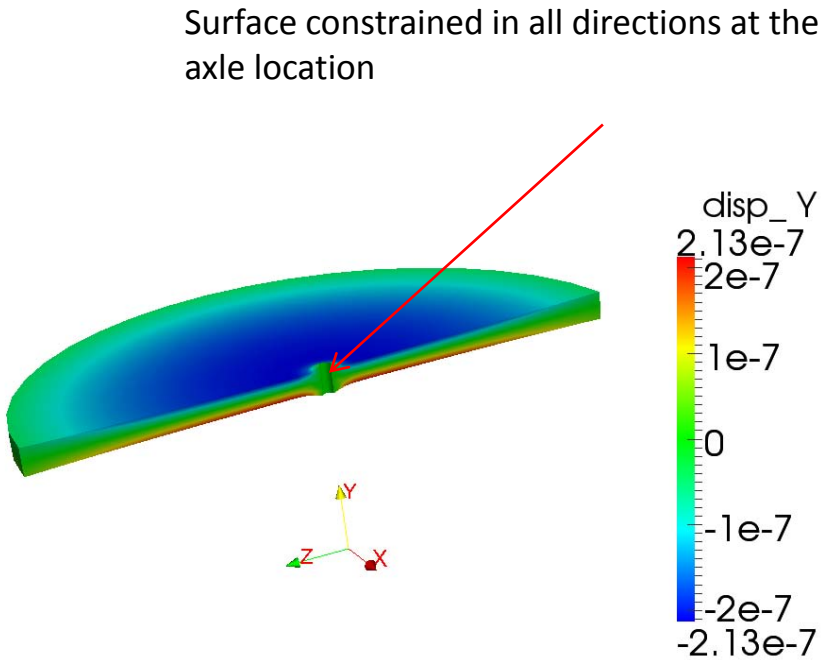

Figure 4 Displacement contour plot of the spinning disk magnified by a factor of 200,000x.

3. IMPELLER DESIGN COMPARISON

Previous and current designs of the impeller are compared in this section. The previous design is referred to as the version 4 design, and the current one is version 5. This comparison serves two purposes. One is to compare the analysis methodology with results previously generated and the second is to compare the results between the two different designs. The previous results were not provided for inclusion in this work, but personal communication from the design team indicates that they are similar to their satisfaction. The geometric definition for each design is shown in Figure 5. The finite element meshes are shown in Figure 6. Material properties and rotational velocities are summarized in Table 1. Resulting contour plots of the lateral deflections are shown in Figure 7, but will hereafter be referred to as "axial" deflections, which is a natural term to fit the geometry of the impeller. The maximum axial deflections as a function of rotational velocity are shown in Figure 8, and the axial deflections as a function of radial position (approximately every 0.25”) are shown in Figure 9. Although the geometry and material properties used in the model are specified in the English inch-pound-second (ips) system, the displacements shown in Figures 8-9 are converted to microns for more direct comparison to the design specification of a 10 micron air bearing gap.

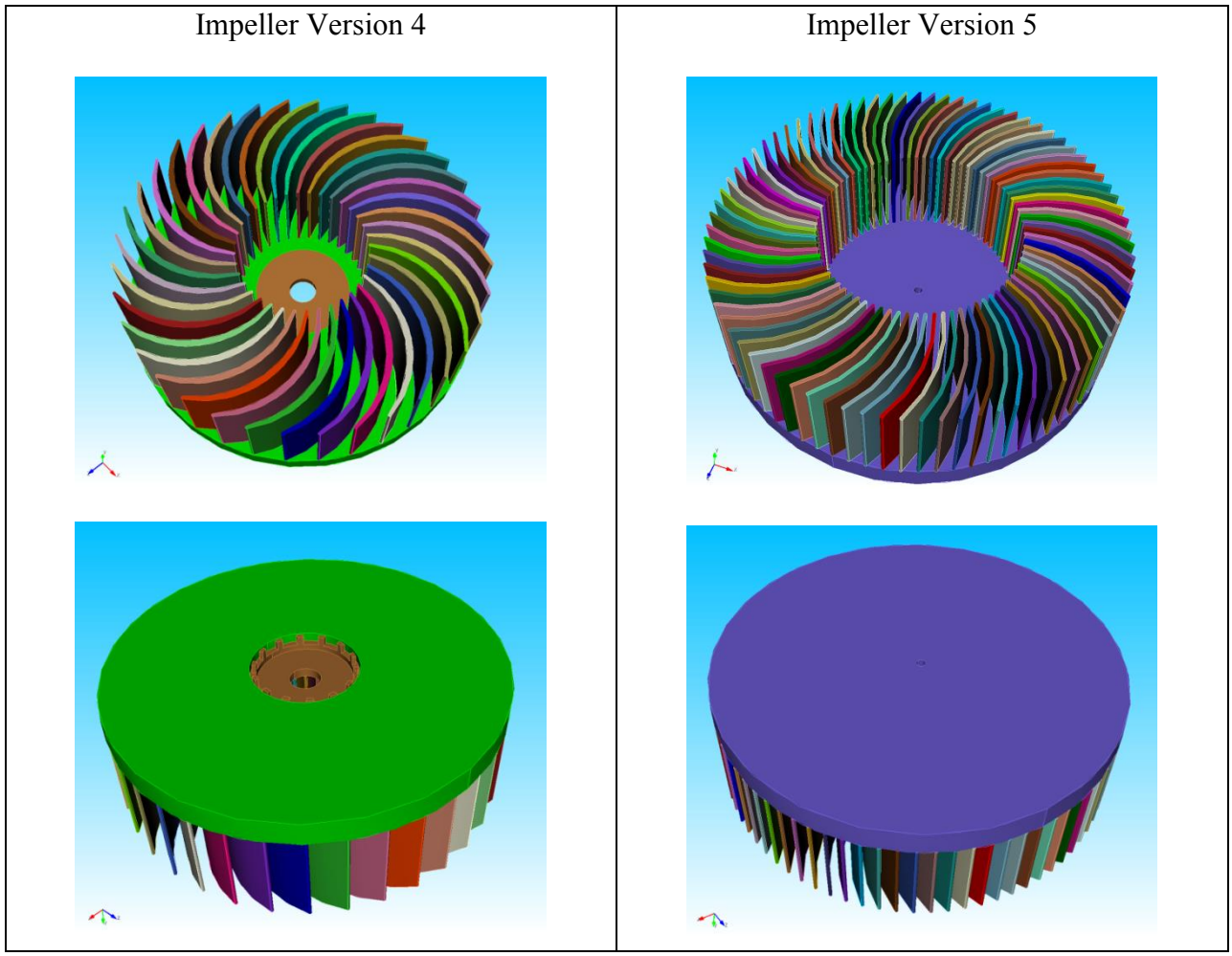

Figure 5 Geometry of the version 4 and version 5 impeller designs.

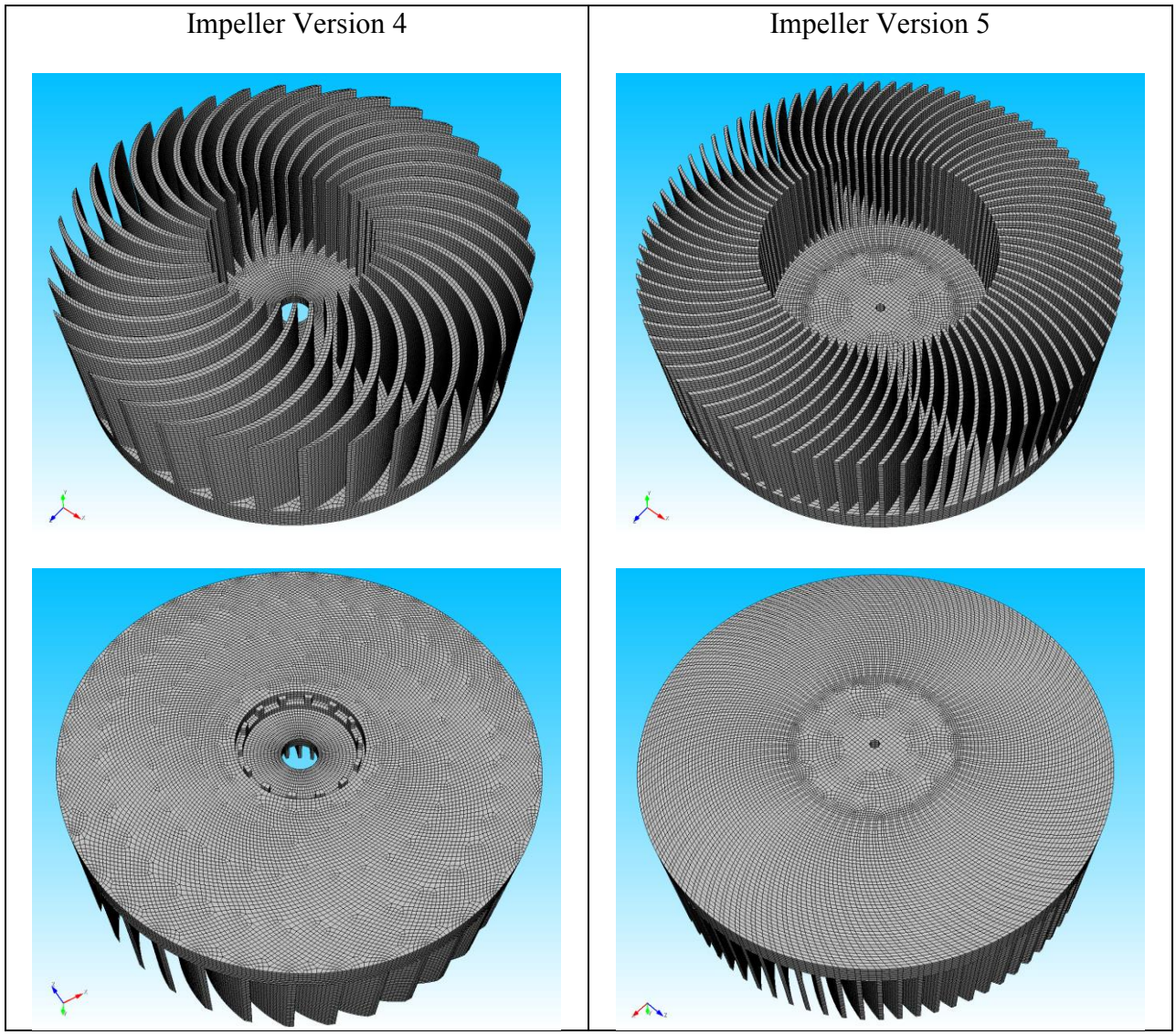

Figure 6 Meshed geometry of the version 4 and version 5 impeller designs.

Table 1 Summary of parameter values used in the comparison between the version 4 and version 5 impellers.

Parameter	**Value**
Elastic Modulus	10×10^6 psi
Poisons Ratio	0.36
Density	2.53×10^{-4} lb·s^2/in^4
Rotational Velocities	1000 to 3000 rpm in 100 rpm increments

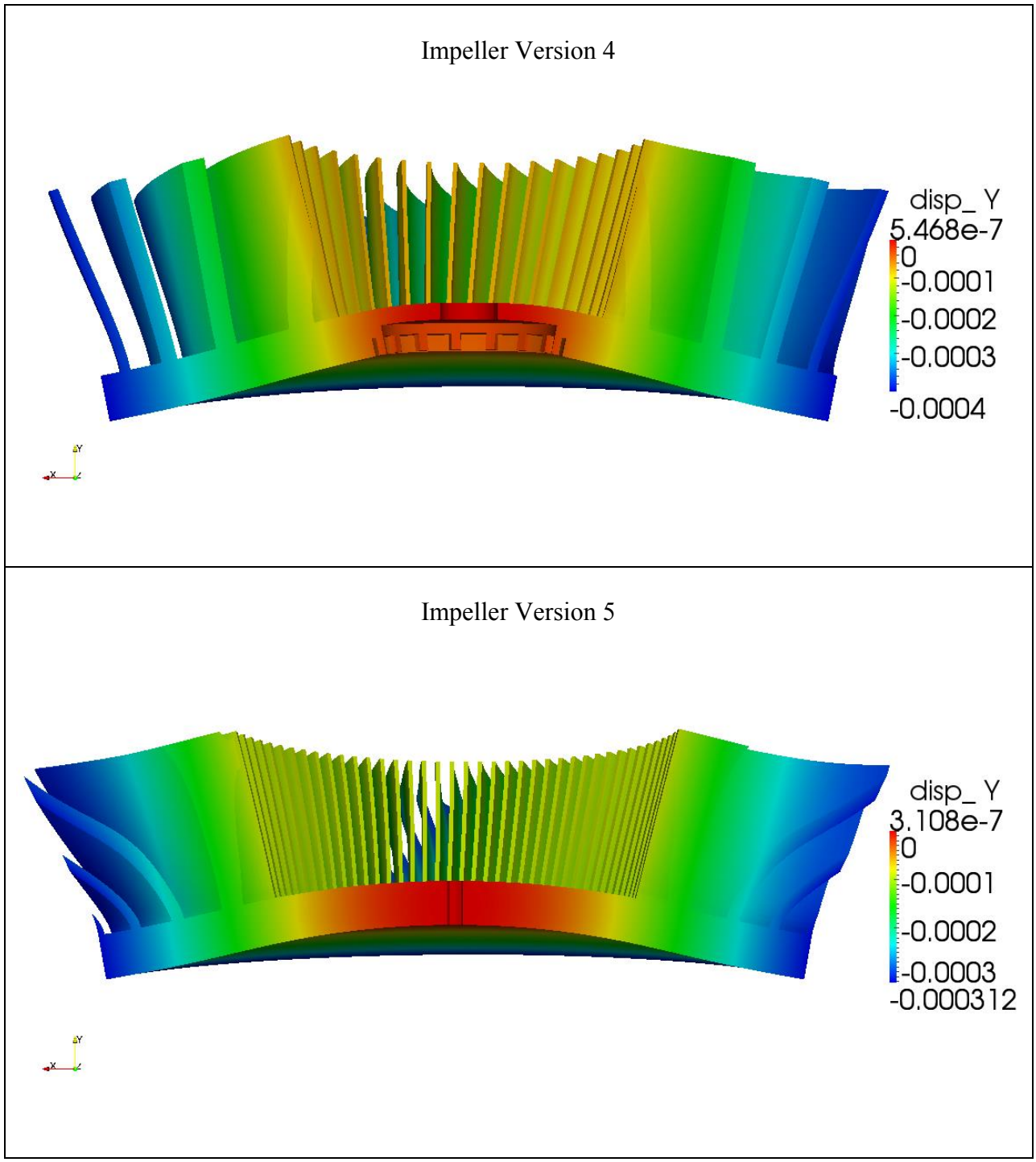

Figure 7 Axial displacement contour plots of the version 4 and 5 impeller designs magnified by a factor of 1000x.

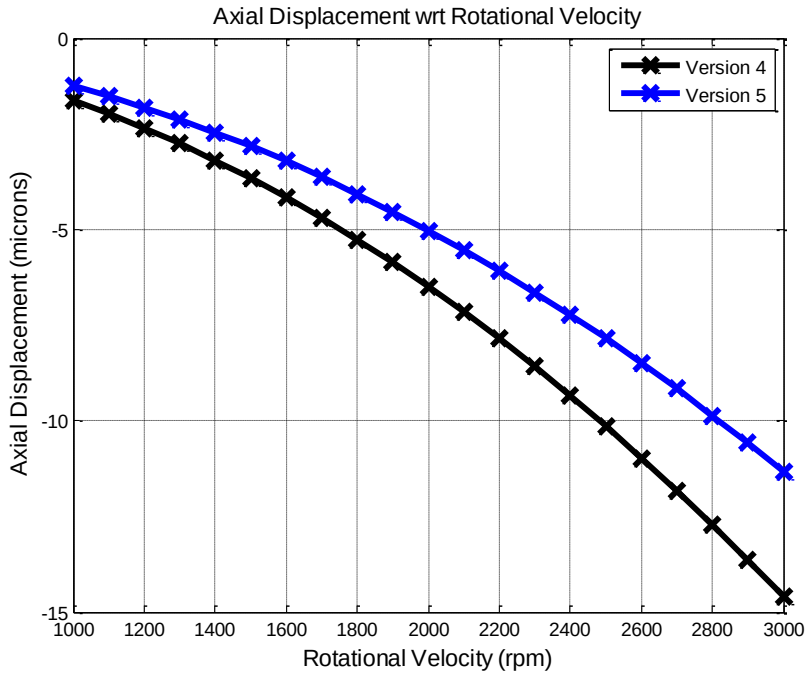

Figure 8 Comparison of the maximum axial displacement as a function of rotational velocity between the version 4 and 5 impellers.

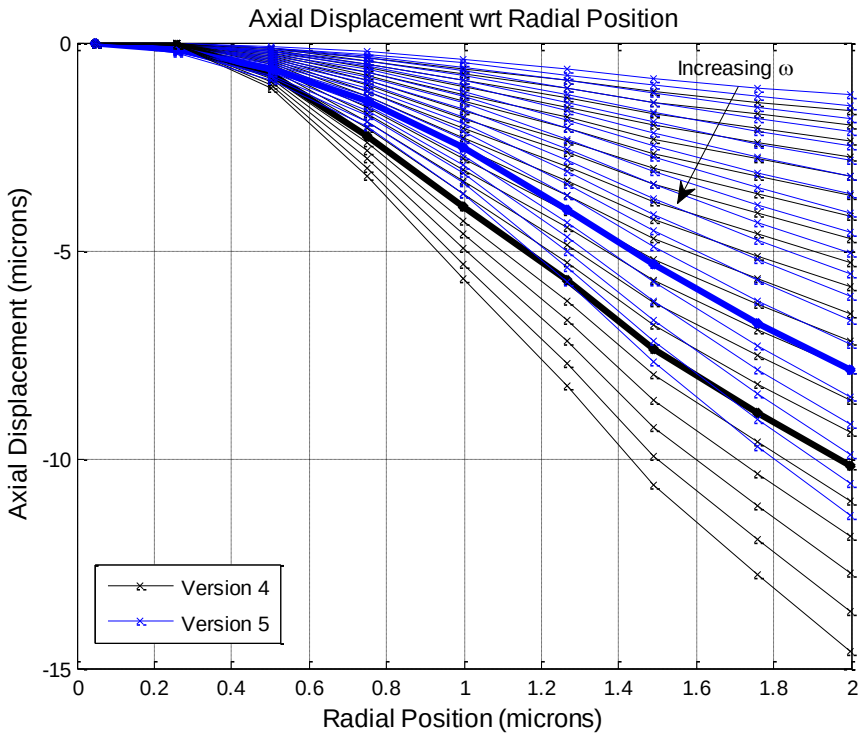

Figure 9 Axial displacements as a function of radial position for both the version 4 and version 5 impellers for rotational velocities ranging from 1000 to 3000 rpm in 100 rpm increments. A rotational velocity of 2500 rpm is emphasized.

4. PARAMETER STUDY

The version 5 impeller geometry was used in a parameter study to investigate how material selection, thickness, and blade pressure influence the observed deflection. The parameters and their assigned values are summarized in Table 2. Ensembles of simulations were in three main steps. The first step ran a full factorial matrix varying the rotational velocities, aluminum or copper selection, and applied blade pressures. Next, the 0.125" and 0.375" disk thicknesses were run, again in a full factorial ensemble varying the rotational velocity with the thicknesses. Finally, a thickness profile tapered with the intent of compensating for the observed "baseline" displacements of the 0.25" aluminum impeller at 2500 rpm was run at all rotational velocities. The results are partially shown in Figure 10. Only one set of rotational velocity curves are shown because they are similar in trends to the other sets. The intent of the figure is to show how the "baseline" case compares to other rotational velocities, pressure loads on the blades, a copper impeller, different disk thicknesses, and finally the tapered cross-sectional profile. Because the thinner impeller disk experiences significant deflection, the axes are rescaled in Figure 11 to capture more detail for the rest of the results.

Table 2 Summary of parameters and values used in the parameter study. Highlighted values are considered as "baseline".

Parameter	**Values**
Rotational velocity	1000 to 3000 rpm in 100 rpm increments (**2500 rpm**)
Pressure on concave side of blade	**0**, -15, -30, -45, -60 Pa
Pressure on top of blade	**0**, 15, 30, 45, 60 Pa
Material property selection	**Aluminum** ($E=10\times10^6$ psi, n = 0.36, density = 2.53×10^{-4} lb·s^2/in^4) Copper ($E=16\times10^6$ psi, n = 0.343, density = 7.43×10^{-4} lb·s^2/in^4)
Disk thickness	0.125", **0.250",** 0.375"
Tapered profile	Linear taper starting at a radial distance of 0.5" and reaching an offset of 0.00031" at the edge (2.0" radial distance).

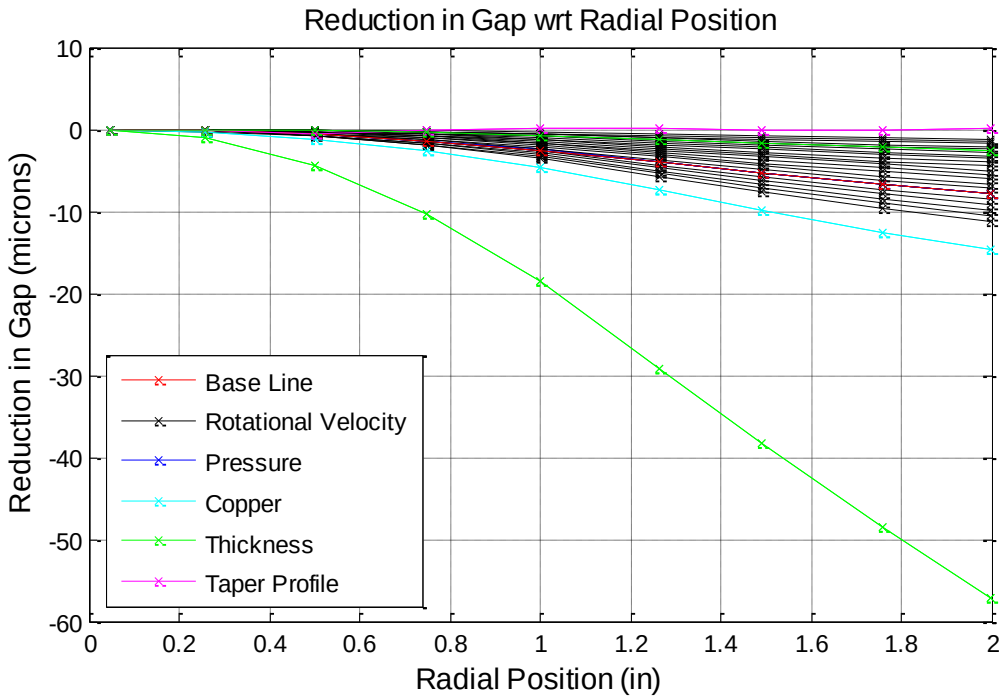

Figure 10 Parameter trends affecting the impeller gap distance.

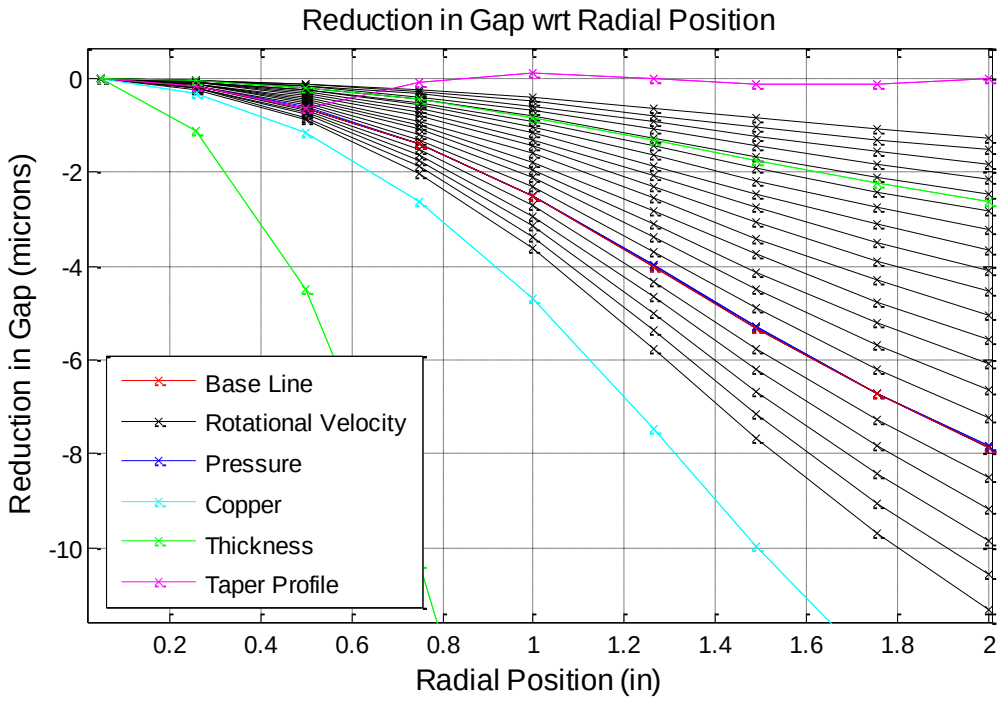

Figure 11 Zoomed in parameter trends.

The observed impact of the different parameter values may be summarized as follows:

1) The applied pressures to the impeller blades have a negligible effect on the deformation of the disk.
2) The choice of aluminum over copper has a significant structural advantage in reducing the amount of axial displacement.
3) The selected thicknesses strongly affect the observed displacements, with the thinner disk undergoing significantly greater axial displacement.
4) Tapering the disk's thickness to account for calculated axial displacement does result in maintaining nearly the entire initial gap of 10 mirons. Some oscillations in the surface are noticed, although they are relatively small, being less than +/-1 micron.

5. SENSITIVITY / ANOVA STUDY

A sensitivity study is performed to provide an indication on how sensitive the axial displacement is to possible variations in the different parameters. Based on the previous work, the selected factors / parameters are the rotational velocity, disk thickness, Poison's ratio, elastic modulus, and density of the material. Three levels / values are used for each factor. The range for each factor is selected with the intent of realistically bounding the values which may be expected during operation and manufacturing. However, additional research or expert opinion was not obtained for each parameter, so the bounds remain an arbitrary estimate at this point. The selected factors and levels are summarized in Table 3, with some explanation for their selection.

Table 3 Factor levels selected for a sensitivity study of the axial displacements.

Factor	Levels	Notes
Rotational Velocity	2475, 2500, 2525 rpm	+/ 1% of 2500 rpm
Disk Thickness	0.248, 0.250, 0.252 in	Thickness manufactured within +/- 2 mil
Poison's Ratio	0.3, 0.33, 0.36	+/- ~10% of 0.33 matweb.com reported values: aluminum: 0.36 aluminum 6061-T6, 6061-T6: 0.33
Elastic Modulus	9.5, 10, 10.5×10^{6} psi	+/- 5% of 10×10^{6} psi matweb.com reported values: aluminum: 9.86×10^{6} psi aluminum 6061-T6; 6061-T6: 10×10^{6} psi aluminum 7075-T6, T651: 10.4×10^{6} psi
Density	2.394×10^{-4}, 2.52×10^{-4}, 2.646×10^{-4} $lb\cdot s^2/in^4$	+/- 5% of 2.52×10^{-4} $lb\cdot s^2/in^4$ matweb.com reported values: aluminum: 2.53×10^{-4} $lb\cdot s^2/in^4$ aluminum 6061-T6, 6061-T6: 2.53×10^{-4} $lb\cdot s^2/in^4$ aluminum 7075-T6, T651: 2.64×10^{-4} $lb\cdot s^2/in^4$

A full factorial design of experiments matrix was evaluated with the selected factors and levels for a total of 243 simulations in this sensitivity study. An analysis of variation (ANOVA) calculation was performed on the maximum axial displacements observed in each simulation. The p-values for the null hypothesis on the main effects were all nearly 0, indicating that each factor was significant in the observed axial displacements (typically $p < 0.05$ indicates significance).

Plots of the displacements as a function of radial position were generated in two ways in order to visualize the impact of each factor. The first way is to plot all the results and color each series either blue, green, or red depending on whether the low, medium, or high value of the selected factor is being displayed. This technique results in a separate plot for each factor, which are shown in Figure 12. It should be noted that the sequence of plotting was for low, then medium, and then high values. Therefore, the red color often covers the green and blue colors. One

insight from these plots is that there are not distinct bands of each color, further indicating that all the factors are significant. Also, the range of displacements due to possible uncertainty in the design parameters is illustrated. The second way the results are displayed is in a similar series of plots which contain only the low, medium, and high values for a single factor while holding the other factors at their medium/nominal target value. Thus the range of displacements due to the single factor is illustrated, as shown in Figure 13.

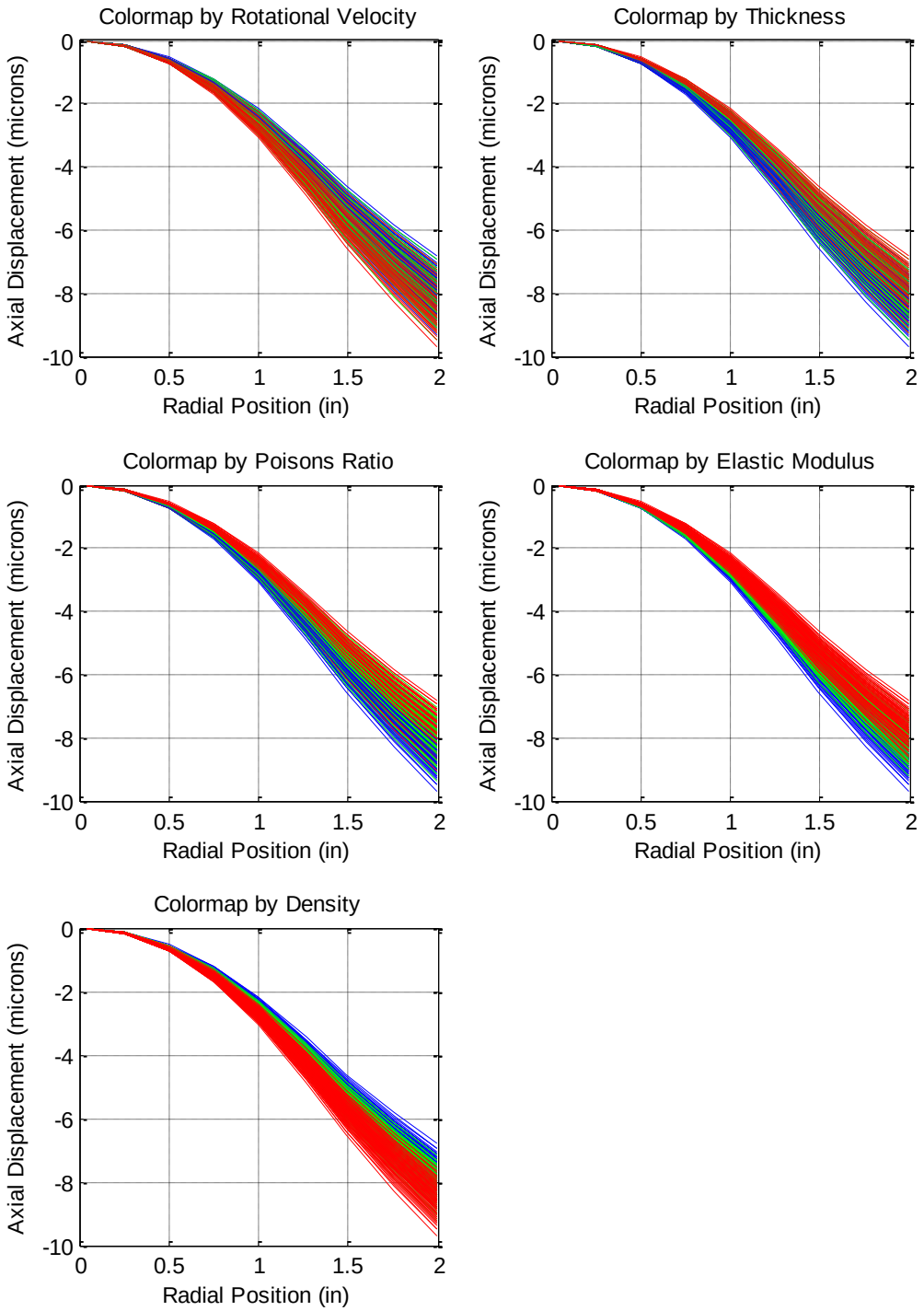

Figure 12 Plots of each factor colored separately by blue, green, or red for low, medium, and high levels.

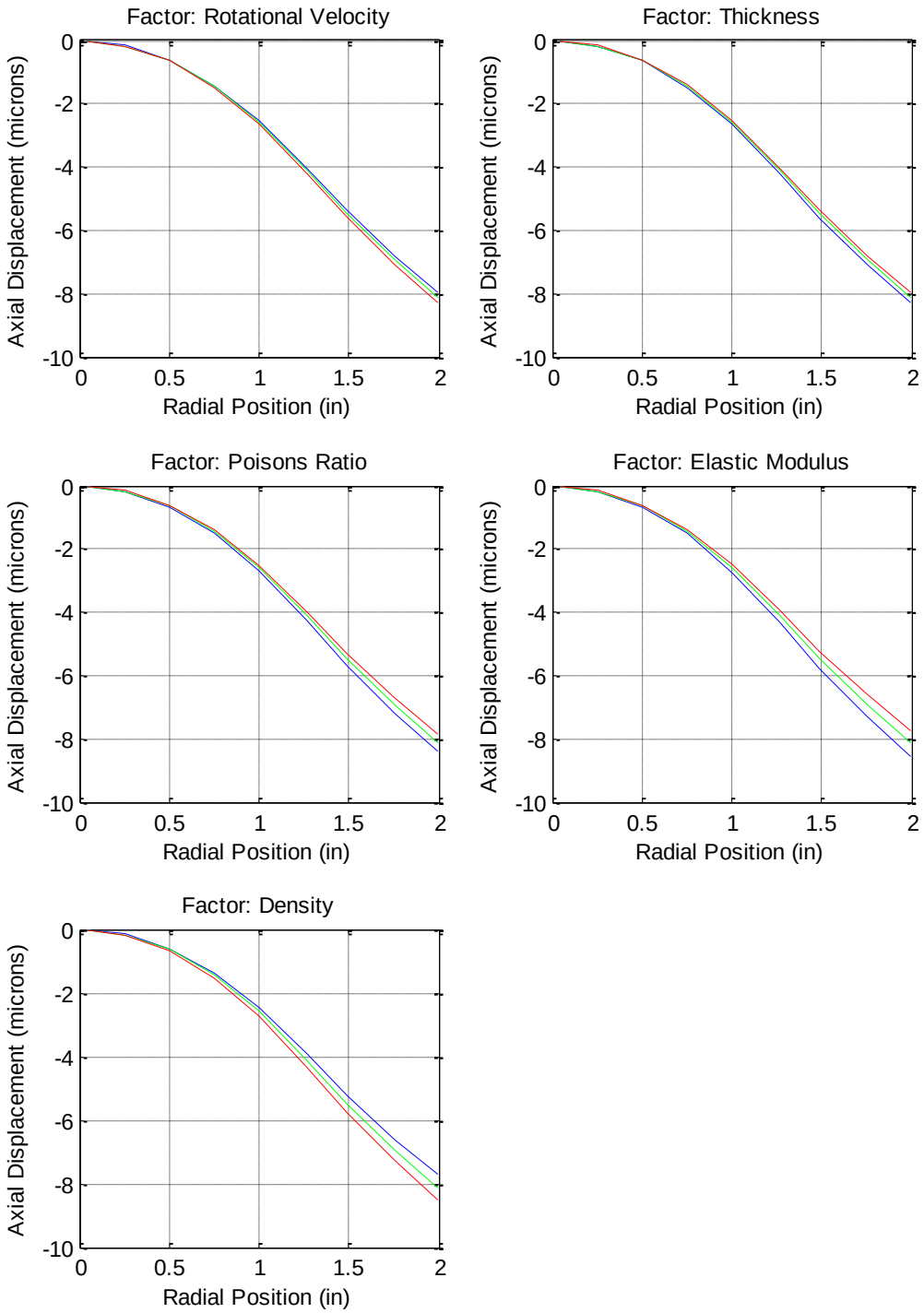

Figure 13 Plots of each factor at their low (blue), medium (green), and high (red) levels with the other factors held constant at their medium/nominal level.

6. MODAL ANALYSIS

The mode shapes and frequencies of the version 5 impeller were calculated using the same finite element meshes and material properties as described in Section 3 with the Sierra Structural Dynamics code [3]. A fixed boundary condition is specified at the nodes on the interior of the impeller's center through hole (contacting surface for the axle shaft). The calculated modes up to about 2600 Hz occur at about 437, 707, 1493, 1682, 2414, 2556, 2586, 2590, and 2598 Hz. The corresponding mode shapes are shown in Figure 14.

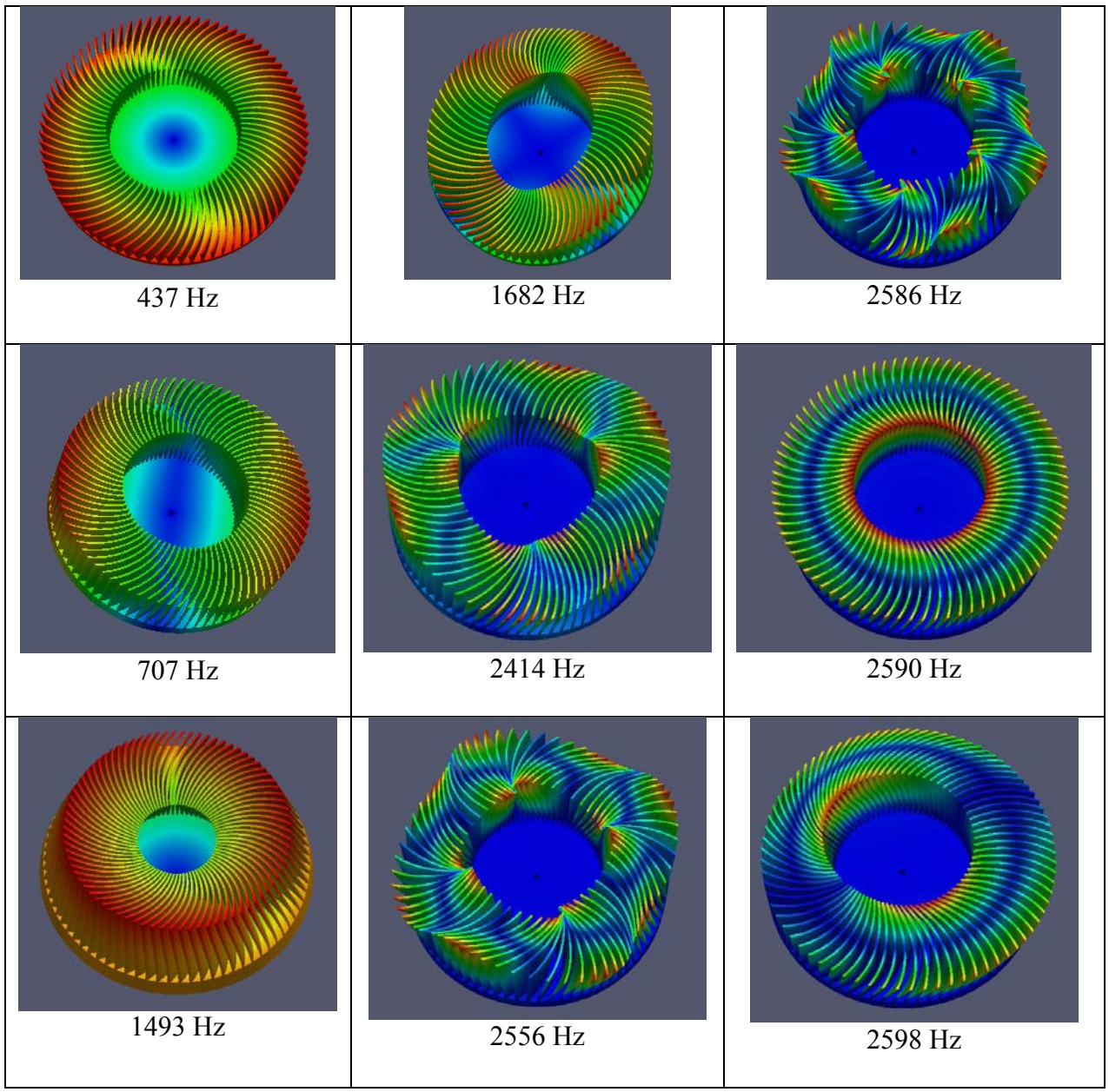

Figure 14 Version 5 impeller mode shapes and corresponding frequencies.

Of particular interest is the mode at 2590 Hz, which is similar in shape to the first mode of an isolated fin with the fixed boundary condition applied where it contacts the spinning disk, as shown in Figure 15. The interest in this particular mode is due to a concern that vibration resulting primarily from fin excitation is responsible for undesirable noise generation at some rotational velocities. Some investigative work was done in changing the fin geometry, designated as version 6, to see its effect on the modal response. The version 6 fin geometry and resulting first mode shape, with the fin base having a fixed displacement, is shown in Figure 16. The natural frequency of this first mode of the version 5 fin is less than the first mode of the version 6 fin at 2699 Hz versus 2989 Hz. However, the mode shapes are different. The first mode of the version 5 fin actually resembles the second mode of the version 6 fin and vice versa. An explanation of this behavior may be attributed to the difference in height and thickness of the fins affecting the mode shape order. It should be noted that while isolating the fins is instructive to their behavior, actual performance will be dependent on the entire device, including the platen, axle, and attachments (as can be seen for the platen and fin case in Figure 14). The relative importance of each part of the entire platen will change depending on the mass and stiffness of each contributing part. For example, as the platen's stiffness increases, then the isolated fin case with a fixed base is approached.

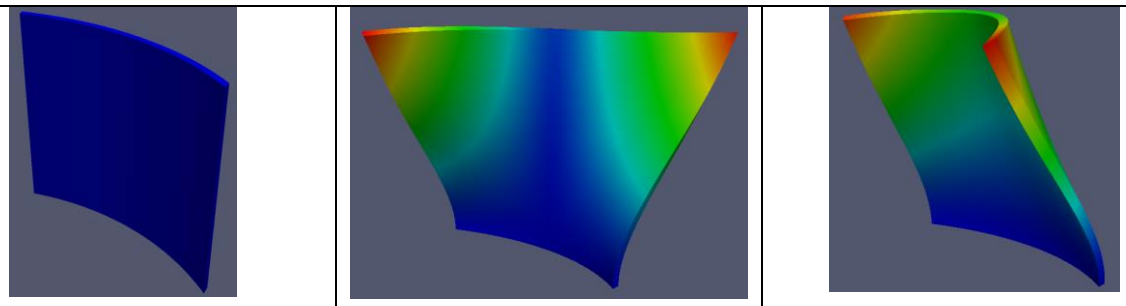

(a) Isolated Fin | (b) First Mode 2699 Hz | (c) Second Mode 3688 Hz

Figure 15 Version 5 (a) isolated fin geometry, (b) first mode, and (c) second mode with the base of the fin having a fixed displacement boundary condition.

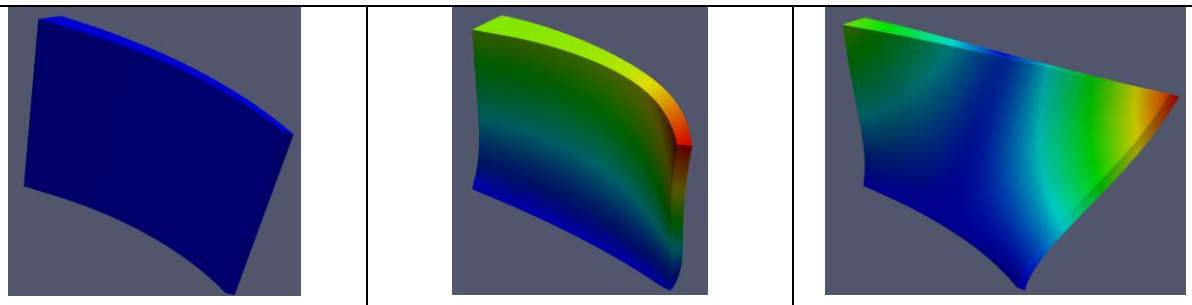

(a) Isolated Fin | (b) First Mode 2989 Hz | (c) Second Mode 3458 Hz

Figure 16 Version 6 (a) isolated fin geometry, (b) first mode, and (c) second mode with the base of the fin having a fixed displacement boundary condition.

7. CONCLUSIONS

The observed maximum axial displacements for the version 5 impeller operating at the target rotational velocity of 2500 rpm are approximately 8 μm, close to the total target air gap of 10 μm. An initial approach of tapering the thickness of the disk to compensate for the axial displacement did result in significantly reduced displacements which oscillated about 0 μm.

Another design consideration is in the manufacturing and operational tolerances of the device. An initial sensitivity study indicated that the axial displacements may vary up to 2.9 μm based upon the selected bounds of considered design parameters. Updated knowledge of the manufacturing tolerances and operation of the device will likely change this possible variation. Other aspects may warrant investigation as well if tight operational tolerances are required.

The finite element modeling procedure and post processing for the different impeller designs continues to be utilized by the impeller design team for performance evaluations. Some design options and considerations that were not reported in the body of this report are included in the Appendix. These include the platen axial displacements of the version 6 impeller, the evaluation of a fin design using pins, and scoping calculations of thermal gradient effects on axial displacements.

8. REFERENCES

[1] "Sierra/Solid Mechanics 4.28 User's Guide," Sandia National Laboratories, Albuquerque, New Mexico 2013.

[2] P. A. Kelly, "Lecture Notes in Solid Mechanics Part II: Engineering Solid Mechanics," ed. Aukland, New Zealand: University of Aukland.

[3] G. Reese, D. Segalman, M. K. Bhardwaj, K. Alvin, B. Driessen, K. Pierson, and T. Walsh, "Salinas -User's Notes," Sandia National Laboratories, Albuquerque, NM SAND99-2801, February 4, 2013.

APPENDIX A: VERSION 6 AXIAL DISPLACEMENTS

The version 6 impeller consists of a fewer number of fins which are thicker and taller. The solid model definition also included different axle attachment geometry. Meshes of the version 5 and 6 meshes are shown below in Figure 17 for comparison. Figure 18 shows a comparison of axial displacements for the three impeller versions reported in this work. It is observed that the axial displacement for the version 6 impeller exceeds the 10 micron threshold at 2500 rpm with the standard 0.25" thick platen. Another set of simulations are run with a 0.375" thick platen, resulting in significantly less axial displacement, which is also shown in Figure 18.

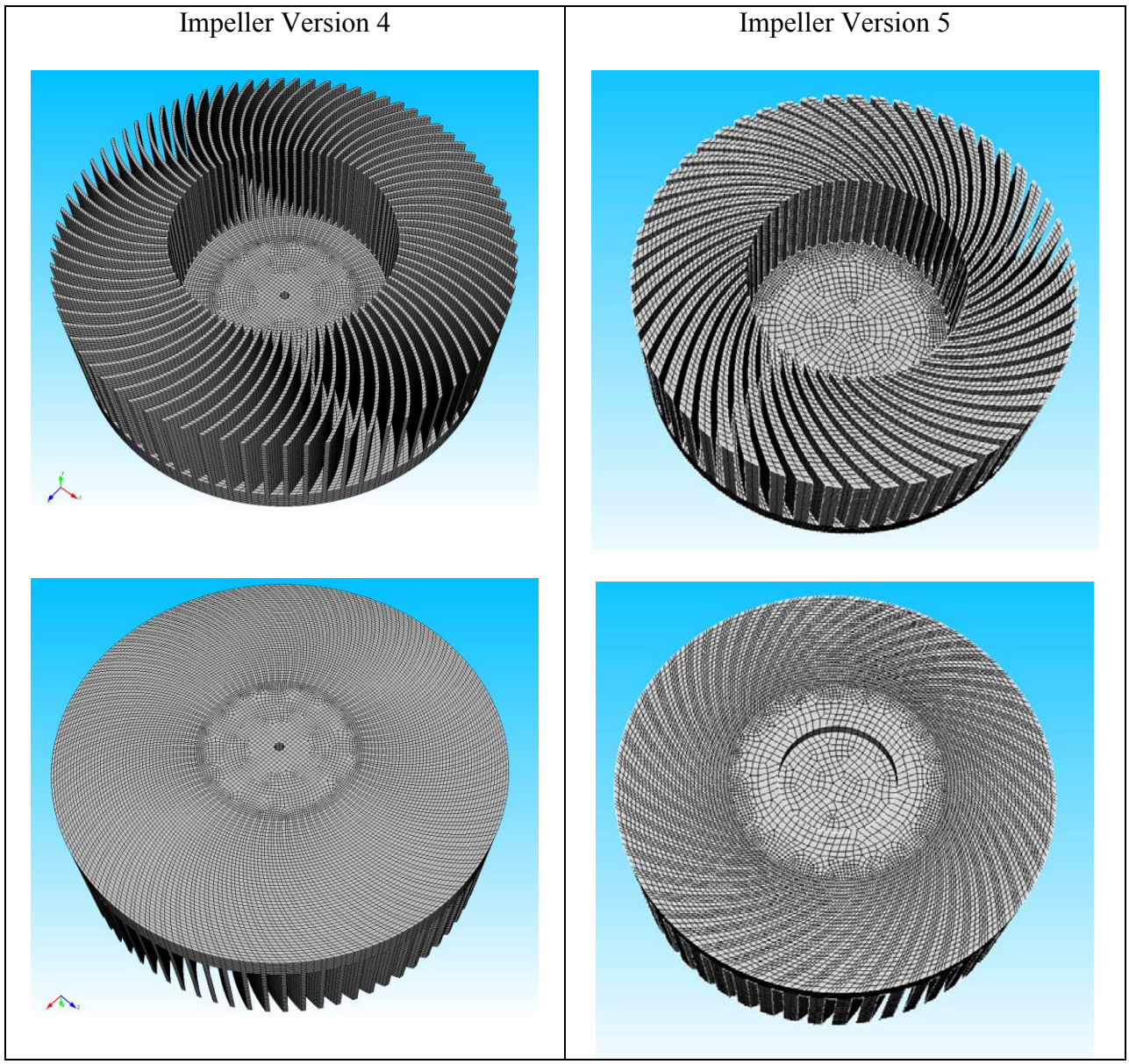

Figure 17 Meshed geometry of the version 5 and version 6 impeller designs.

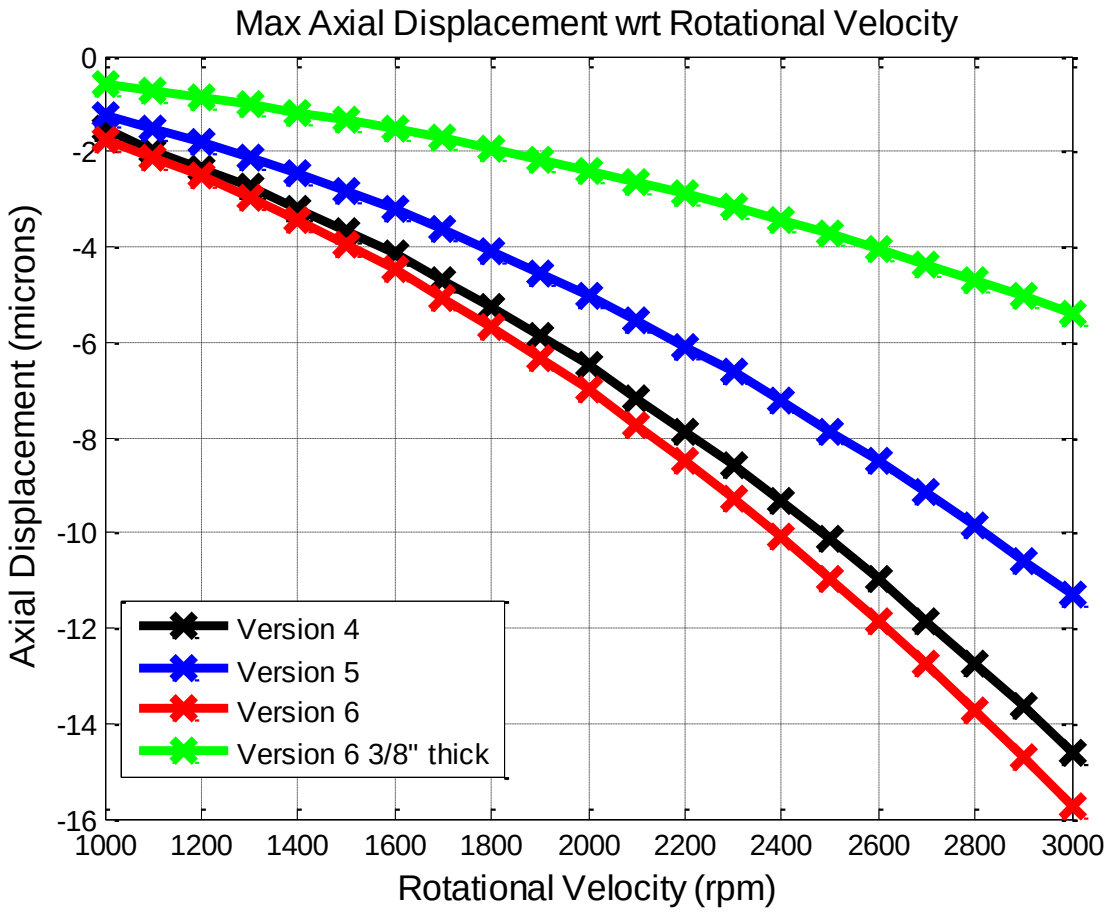

Figure 18 Maximum axial displacements overlaid with the version 6 impeller design.

APPENDIX B: IMPELLER PIN DESIGN

An impeller design using fins consisting of pins was simulated to explore the new concept. The mesh of the pin impeller is shown in Figure 19, followed by radial displacements in Figure 20.

Impeller Pin Conceptual Design

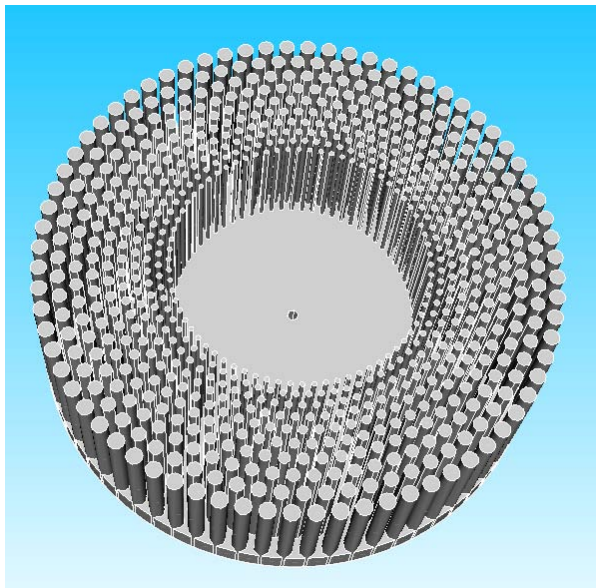

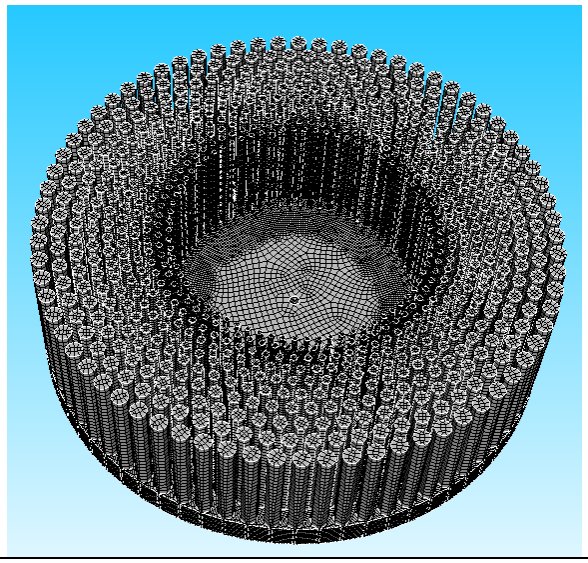

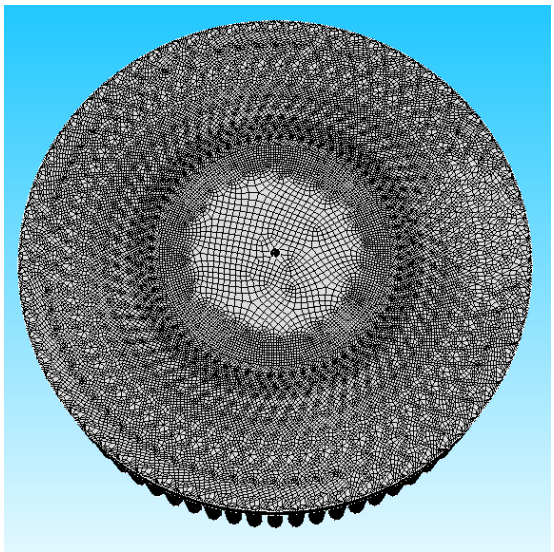

Figure 19 Meshed geometry of conceptual impeller design with pins forming the fins.

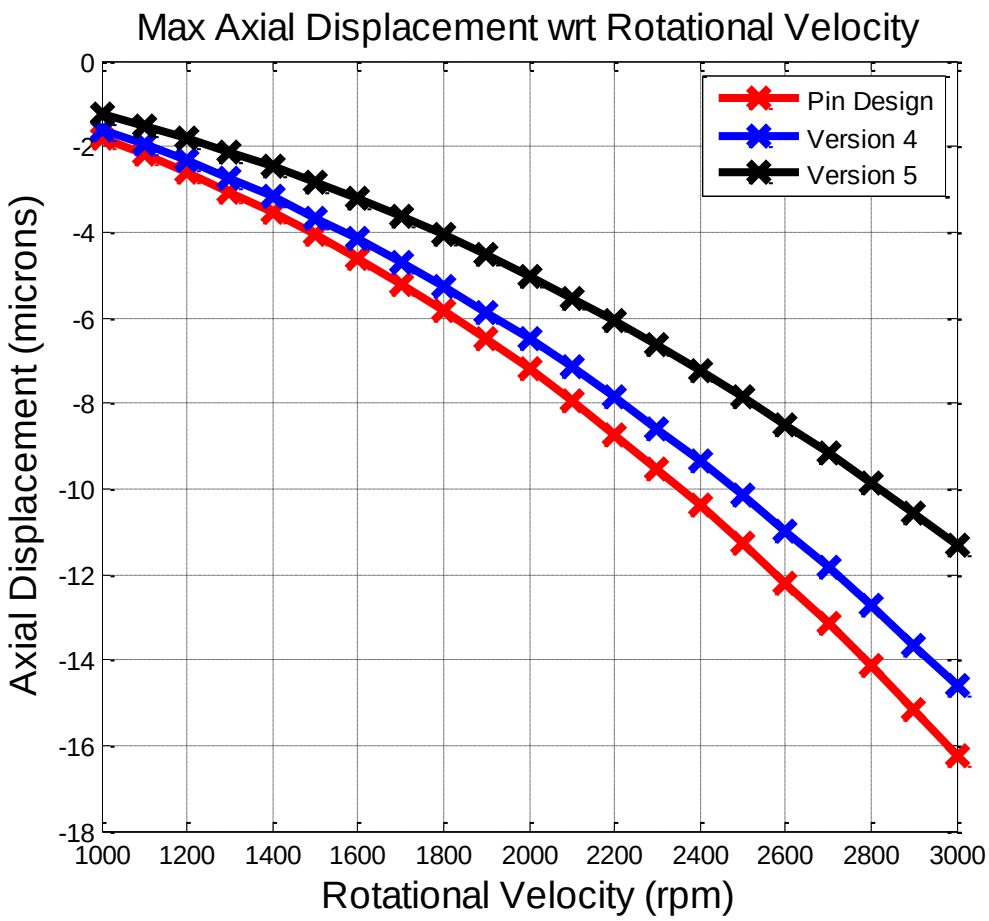

Figure 20 Maximum axial displacements overlaid with the pin fin impeller design.

APPENDIX C: THERMAL GRADIENT DISPLACEMENTS

A thermal gradient due to the cooling process of the impeller fins was applied to the version 5 impeller based on a temperature distribution provided by a separate thermal modeling effort. This temperature distribution was provided along a line path, consisting of x, y, and z coordinates with a corresponding temperature. Temperatures were then assigned based on this path in discrete sections of the impeller and made axisymmetric. The resulting temperature distribution and displacement due to thermal strains is shown in Figure 21. Although the temperature distribution is based on a relatively crude mapping, the temperature differences are not very large. Therefore, for design scoping purposes a finer temperature distribution was not pursued at this time. A line plot of the axial displacements as a function of radial position is shown in Figure 22. Based on these results, it is deemed important to consider the platen displacements due to the operational thermal gradient of the cooler.

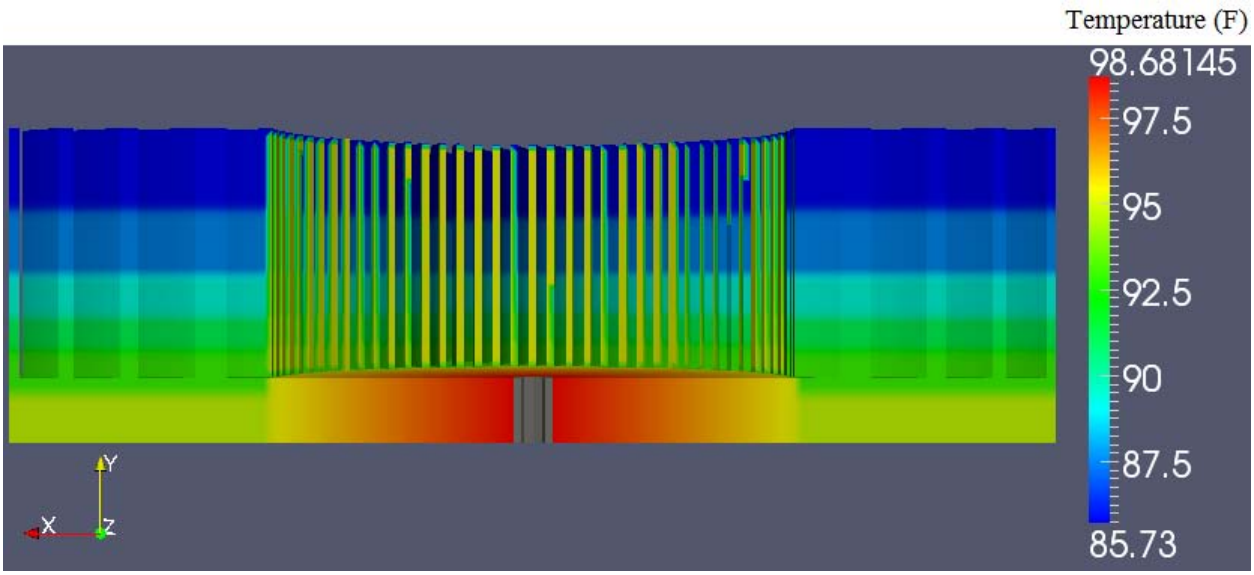

(a)

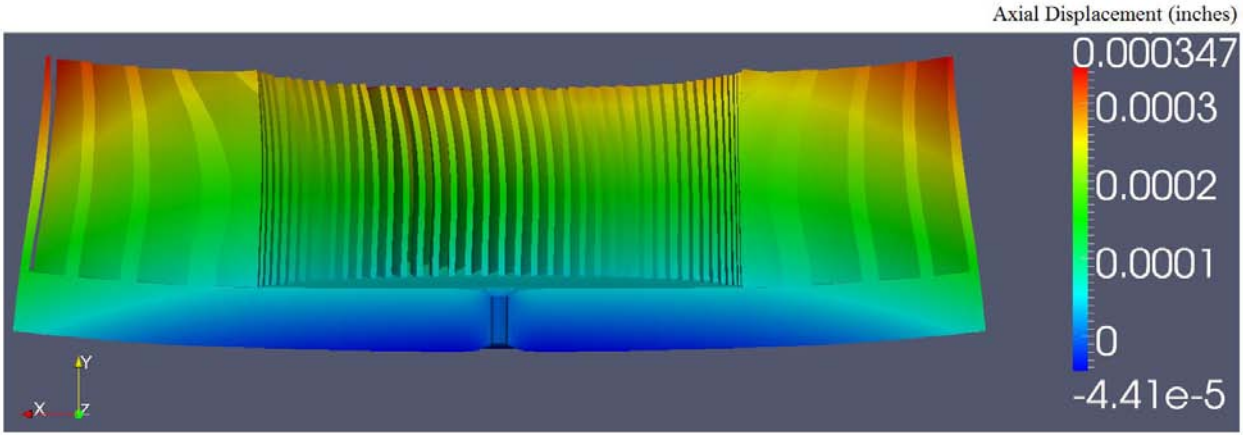

(b)

Figure 21 Version 5 (a) mapped temperature distribution and (b) resulting axial displacements.

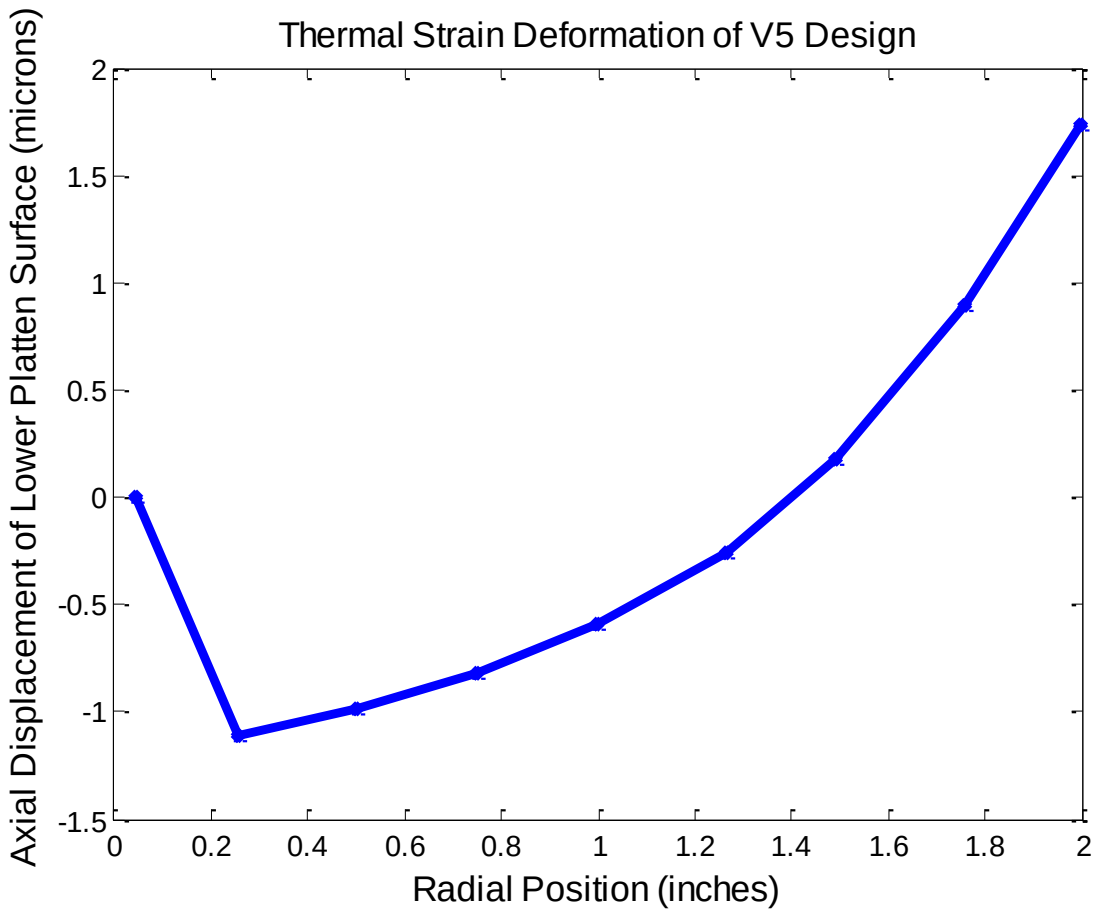

Figure 22 Axial displacements of the version 5 impeller due to thermal gradients during the operational cooling process for one calculated temperature distribution.

DISTRIBUTION

1	MS9014	Dita Curgus	8366
1	MS9042	Mary Gonzales	8250
1	MS9042	Mike Chiesa	8259
1	MS9042	Nathan Spencer	8259
1	MS9051	Imane Khalil	8366
1	MS9051	Daniel Matthew	8366
1	MS9051	Wayne Staats	8366
1	MS9052	Marco Arienti	8365
1	MS9056	Jeff Koplow	8366
1	MS9402	Terry Johnson	8366
1	MS9409	Michael Leick	8366
1	MS9957	Patricia Gharagozloo	8365
1	MS0899	Technical Library	9536
1	MS9018	Central Technical Files	8944

Sandia National Laboratories